Published in final edited form as:
Matrix Biol. 2013 April 24; 32(0): 196–207. doi:10.1016/j.matbio.2013.02.002.

Biochemical and biophysical changes underlie the mechanisms of basement membrane disruptions in a mouse model of dystroglycanopathy

Peng Zhang[*], **Yuan Yang**[*,#], **Joseph Candiello**[†], **Trista L. Thorn**[*], **Noel Gray**[*], **Willi M. Halfter**[‡], and **Huaiyu Hu**[*,§]

[*]Department of Neuroscience and Physiology, SUNY Upstate Medical University

[#]Department of Neurology and Psychiatry, Tongji Hospital, Tongji Medical College, Huazhong University of Science and Technology, Wuhan, P.R. China

[†]Department of Biomedical Engineering, University of Pittsburg

[‡]Department of Neurobiology and Anatomy, University of Pittsburg

Abstract

Mutations in glycosyltransferases, such as protein O-mannose N-acetylglucosaminyltransferase 1 (POMGnT1), causes disruptions of basement membranes (BMs) that results in neuronal ectopias and muscular dystrophy. While the mutations diminish dystroglycan-mediated cell-ECM interactions, the cause and mechanism of BM disruptions remain unclear. In this study, we established an *in vitro* model to measure BM assembly on the surface of neural stem cells. Compared to control cells, the rate of BM assembly on POMGnT1 knockout neural stem cells was significantly reduced. Further, immunofluorescence staining and quantitative proteomic analysis of the inner limiting membrane (ILM), a BM of the retina, revealed that laminin-111 and nidogen-1 were reduced in POMGnT1 knockout mice. Finally, atomic force microscopy showed that the ILM from POMGnT1 knockout mice was thinner with an altered surface topography. The results combined demonstrate that reduced levels of key BM components cause physical changes that weaken the BM in POMGnT1 knockout mice. These changes are caused by a reduced rate of BM assembly during the developmental expansion of the neural tissue.

Keywords

basement membrane; dystroglycanopathy; retina; laminin; extracellular matrix; POMGnT1

1. Introduction

Congenital muscular dystrophies (CMDs) associated with malformations of the central nervous system are frequently caused by mutations in glycosyltransferases including *POMT1* (Beltran-Valero de et al., 2002;Currier et al., 2005); *POMT2* (van Reeuwijk et al., 2005); *POMGnT1* (Yoshida et al., 2001); *LARGE* (Longman et al., 2003); *FKTN* (de

[§]Address correspondence to: Huaiyu Hu, Department of Neuroscience and Physiology, SUNY Upstate Medical University, 750 E. Adams Street, Syracuse, NY 13210 USA. Phone: 315-464-8143. Fax: 315-464-7712, huh@upstate.edu.

Bernabe *et al.*, 2003;Kobayashi *et al.*, 1998); and *FKRP* (Beltran-Valero de *et al.*, 2004;Brockington *et al.*, 2001). Recently, mutations in collagen IV α1 (COL4A1) (Labelle-Dumais *et al.*, 2011) and ISPD (encoding isoprenoid synthase domain containing) (Roscioli *et al.*, 2012;Willer *et al.*, 2012) are identified as new causes. *POMT1* and *POMT2* encode protein O-mannosyltransferase 1 and 2, which form a mutually indispensible enzyme complex to initiate synthesis of O-mannosyl glycosylation on glycoproteins (Manya et al., 2004). Protein O-mannose β-1,2 N-acetylglucosaminyltransferase 1, encoded by *POMGnT1*, transfers N-acetylglucosamine to the existing O-mannose forming a β-1,2 extension (Yoshida et al., 2001). Like-glycosyltransferase (LARGE) exhibits xylosyl- and glucuronyl- dual transferase activities and generate repeating disaccharide units of [–3-xylose–α1,3-glucuronic acid-β1–] (Inamori *et al.*, 2012). The precise biochemical functions of the protein products of *FKTN* and *FKRP* (fukutin and fukutin-related protein) are not known.

An important target of these glycosyltransferases is α-dystroglycan (α-DG), a cell surface ECM receptor that is a key component of the dystrophin glycoprotein complex. At the cell surface, α-DG binds to laminin (Ervasti and Campbell, 1993;Gee *et al.*, 1993;Smalheiser and Kim, 1995;Yamada *et al.*, 1994), agrin (Gee et al., 1994;Yamada et al., 1996), perlecan (Peng *et al.*, 1998;Talts *et al.*, 1999a), neurexin (Levi *et al.*, 2002;Sugita *et al.*, 2001), and pikachurin (Kanagawa et al., 2010) and bridges the ECM to the actin cytoskeleton. Mutations in CMD lead to hypoglycosylation of α-DG, which diminishes its ability to bind these ECM proteins (Grewal *et al.*, 2001;Hu *et al.*, 2011b;Kanagawa *et al.*, 2010;Kano *et al.*, 2002;Kim *et al.*, 2004;Liu *et al.*, 2006;Michele *et al.*, 2002;Takeda *et al.*, 2003). Thus, these diseases are also referred to as dystroglycanopathies.

A hallmark in dystroglycanopathies is a defective pial BM which is the cause of neuronal ectopias in neocortex (Hu et al., 2007;Yamamoto et al., 1997), cerebellum (Li et al., 2008), and hippocampus (Li *et al.*, 2011). Moreover, the inner limiting membrane (ILM), a BM of the retina is disrupted (Ackroyd et al., 2011;Hu et al., 2010;Lee et al., 2005;Satz et al., 2008). Additionally, DG (Williamson et al., 1997), POMT1 (Willer et al., 2004), and POMT2 (Hu et al., 2011a) null embryos die due to disruptions in Reichert's membrane, an extra-embryonic BM. Recently, we found that the ILM in POMGnT1 knockout mice exhibited a significantly reduced Young's modulus (Hu et al., 2010), indicating that mechanical weakness contributes to disruptions of the BMs. However, it is unknown why the mutant ILMs are weakened.

Assembly of the BM is regulated by ECM receptors including integrins and DG (Li et al., 2003). It is conceivable that a diminished interaction between DG and laminin leads to a reduced assembly of BMs. To test this hypothesis, the assembly of BM proteins on POMGnT1 knockout and control neural stem cells was recorded and compared. Further, relative levels of four BM major components of the ILM were compared between POMGnT1 knockout mice and wildtype controls by immunofluorescence staining and quantitative proteomics. Finally, physical properties of POMGnT1 knockout ILM were analyzed by atomic force microscopy (AFM). Our results showed that the assembly rate of ECM on POMGnT1 knockout cells was reduced and that the ILM of POMGnT1 knockout mice showed changes in the biochemical composition and physical structure.

2. Results

2.1. POMGnT1 knockout does not affect membrane localization of DG in radial glial cells and cultured neural stem cells

Deletion of DG in the brain results in disruptions of the pial BM (Moore et al., 2002). One possible cause of BM disruption in POMGnT1 knockout mice could be a defective

localization of DG. To test this possibility, a plasmid pCAG-DG-EGFP, in which EGFP was linked to C-terminus of β-DG, was electroporated into the neocortical wall of POMGnT1 knockout embryos at E13.5. One day after electroporation, green fluorescence in the wildtype was observed throughout the entire radial glial cells reaching the pial surface (Figure 1A). In POMGnT1 knockout neocortical wall, the distribution of green fluorescence was similar to that of wildtype, indicating that DG was transported normally (Figure 1B). Moreover, GFP positive radial glial processes extended through the disruptions of the pial BM beyond pial surface (dashed line in Figure 1B) consistent with previous reports (Hu et al., 2007).

Because radial glial cells are neural stem cells, we isolated neural stem cells from E13.5 POMGnT1 knockout and control embryos and transfected with pCAG-DG-EGFP. These cells expressed the neural stem cell marker nestin (Supplementary Figure 1A and *B*). POMGnT1 knockout neural stem cells exhibited diminished glycosylation and laminin binding as expected (Supplementary Figure 1C and D). However, the GFP fluorescence patterns were indistinguishable between wildtype (Figure 1C, D, and E) and knockout cells (Figure 1F, G, and H), indicating that POMGnT1 knockout does not affect membrane localization of DG. To confirm this, we biotinylated plasma membrane proteins. The biotinylated proteins were isolated by avidin-beads. β-DG immunoblotting showed equal levels of DG immunoreactivity in the membrane fractions of WT and POMGnT1 knockout neural stem cells (Figure 1I). As a control, immunoblotting with antibodies against plasma membrane marker Na^+-K^+-ATPase (Figure 1J) and cytoskeleton protein tubulin (Figure 1K) showed that the avidin-agarose isolated samples were highly enriched for plasma membrane proteins. These results indicate that POMGnT1 knockout does not affect membrane expression of DG.

Deletion of basement membrane components such as perlecan results in disruptions of the pial BM in mice (Costell et al., 1999). A possible cause of the BM disruptions in POMGnT1 knockout mice could be that POMGnT1 deficiency affected the synthesis of ECM. However, the levels of all four major components of the pial basement membrane, including laminin-111, collagen IV, nidogen-1, and perlecan, were indistinguishable between POMGnT1 knockout and control mice (Supplementary Figure 2). In agreement with this, immunoblotting of laminin-111 (Supplementary Figure 2J), nidogen-1 (Supplementary Figure 2K) and perlecan (Supplementary Figure 2H) from total brain lysates did not show significant changes between WT and POMGnT1 knockout mice (Supplementary Figure 2J).

2.2. Rate of laminin assembly was reduced in POMGnT1 knockout neural stem cells

Hypoglycosylation of DG following the deletion of POMGnT1 significantly diminished its ability to bind extracellular ligands such as laminin-111 (Liu et al., 2006). This could lead to a reduced rate in ECM assembly. We therefore performed a laminin assembly assay with POMGnT1 knockout and control neural stem cells. Untreated neural stem cells expressed very low levels of laminin-111 (Supplementary Figure 3A and B). However, substantial laminin binding was observed on the surface of wildtype neural stem cells after incubation with exogenous laminin-111 (Figure 2A). By contrast, a reduced amount of bound laminin was detected on POMGnT1 knockout cells (Figure 2B). Overexpression of POMGnT1 in wildtype neural stem cells by infection with an adenoviral vector Ad-POMGnT1-EGFP did not change the amount of bound laminin-111 (Figure 2E). However, laminin-111 binding was restored to the wildtype levels in POMGnT1 deficient cells after infection with Ad-POMGnT1-EGFP (Figure 2F). To confirm these results, bound laminin-111 was quantified in triplicate experiments by measuring fluorescence intensities and evaluated by a non-linear curve fitting with GraphPad Prism 5 (Figure 2I). While the maximal fluorescence intensity was 4.853 Arbitrary Units for the wildtype neural stem cells, the maximal intensity for POMGnT1 knockout neural stem cells was reduced (2.073 Arbitrary Units, Table I). The

incubation time to reach 50% maximal fluorescence intensity was greater for POMGnT1 knockout neural stem cells (5.046 hour) as compared to wildtype cells (0.545 hour). The results also showed that the initial rate of laminin-111 fluorescence increase (mean ± SEM of 0.859 ± 0.214 Arbitrary Units/hour) was reduced for POMGnT1 knockout cells as compared to wildtype (5.605 ± 0.896 Arbitrary Units/hour, $p<0.001$, F test). Maximal binding, $T_{1/2}$ to reach maximal binding, and initial rate of fluorescence increase were restored to wildtype levels in POMGnT1 knockout cells by infection with Ad-POMGnT1-EGFP virus. As expected, IIH6C4 immunoreactivity in POMGnT1 knockout cells was also rescued by Ad-POMGnT1-EGFP (Figure 2J). Real-time PCR indicated that Ad-POMGnT1-EGFP-treatment resulted in a level of POMGnT1 mRNA at 102.54-fold over the untreated wildtype. However, its overexpression only restored glycosylation of α-DG to the wildtype level.

In addition to the binding assays using monolayer cell cultures, we carried out laminin binding experiments using neural spheres (Figure 3). In a time-course study with wildtype neural stem cell spheres, laminin-111 binding increased from 15 min to 12 hrs of incubation (Figure 3A–F). By contrast, laminin-111 binding on POMGnT1 knockout neural spheres was significantly reduced at all time points (Figure 3A′–F′). To quantify this effect, we measured fluorescence intensities on the sphere surface, size of aggregate, total aggregate area and individual aggregate fluorescence intensity. POMGnT1 knockout neural spheres exhibited decreased overall immunofluorescence intensities (Figure 3G), average size of aggregates (Figure 3H), average immunofluorescence intensity per aggregate (Figure 3I), and area occupied by the aggregates on the sphere surface (Figure 3J). We used a non-linear curve fitting with GraphPad Prism 5 to calculate the maximal fluorescence intensity, time to reach 50% maximal intensity, and initial rate of fluorescence increase (Figure 3G). All three parameters were reduced in POMGnT1 knockout neural stem cell spheres (Table I). The initial rate of laminin-111 immunofluorescence for wildtype neural stem cells was 14.76 ± 1.772 Arbitrary Units/hour. By contrast, the initial rate for POMGnT1 knockout neural stem cells was 5.124 ± 0.926 Arbitrary Units/hour ($p = 0.002$, F test). These results indicate that POMGnT1 deficiency results in a reduced binding of laminin to the surface of neural stem cells. Nevertheless, bound laminin on the surface of both WT and POMGnT1 knockout neural stem cells was mostly co-localized with DG, one of the major cellular receptors of laminin in these cells (Supplementary Figure 3C and D). Therefore, the reduced laminin assembly is likely caused by the impaired function of DG due to hypoglycosylation in POMGnT1 deficiency.

2.3. Formation of a basement membrane-like structure on cultured neural stem cells

Laminin-111 is a key molecule of BMs, facilitating the incorporation of other BM components including collagen IV, nidogen-1, and perlecan (Yurchenco and Wadsworth, 2004). To evaluate BM assembly in an in vitro system, we incubated neural spheres from control wildtype mice with Matrigel, a solubilized preparation of BM. The neural spheres were then stained with antibodies against laminin-111, collagen IV, nidogen-1, and perlecan. Double immunofluorescence staining of laminin-111 (green fluorescence, Figure 4A, B, and C) with collagen IV (Figure 4D), nidogen-1 (Figure 4E), and perlecan (Figure 4F) revealed that laminin-111 was co-localized with the other three BM proteins (merged channels are shown in Figure 4G, H, and I). The co-localization of all four BM proteins suggested the assembly of a complete BM. Transmission electron microscopy was carried out to confirm the formation of a BM. It revealed a thin and uniform electron dense ECM layer on the surface of the neural stem cell plasma membrane that resembled a structurally complete BM *in vivo* (arrows in Figure 4K and L). We also found that 10.79% of plasma membrane length was covered by such electron dense structure. No such structure was observed in neural stem cell cultures incubated without Matrigel (Figure 4J). We did not observe such structure on

POMGnT1 knockout neural stem cells incubated with Matrigel under the same condition (data not shown), which is likely due to dramatically reduced formation of such structures. These results indicate that the ECM aggregates on neural stem cells after incubation with Matrigel form basement membrane-like structure.

To determine whether collagen IV or nidogen alone bind and aggregate on the neural sphere surface, neural spheres were incubated with purified nidogen-1 or collagen IV. Results showed that incubation with collagen IV alone (Figure 4P) did not result in detectable collagen IV binding, and incubation with nidogen-1 resulted in low but detectable binding (Figure 4R). By contrast, incubation with laminin-111 resulted in laminin aggregation on the surface of neural sphere (Figure 4N). These results indicate that the binding of collagen IV and nidogen-1 to neural spheres in Matrigel assembly assay requires the co-binding with laminin.

Co-localization of laminin-111 and collagen IV on the assembled BM could occur in two alternative ways, namely pre-assembly of laminin-111 and collagen IV in solution followed by binding of the complex to the cell surface, or assembly of the proteins at the cell surface in sequence. To determine whether aggregates of laminin, collagen IV, nidogen, and perlecan on neural sphere formed in solution, glycoproteins from wildtype mouse brain, including α-dystroglycan, were isolated, separated on SDS-PAGE, and transferred onto PVDF membranes. The membranes were overlayed with Matrigel and Matrigel protein binding was detected with anti-laminin-111(Figure 4S), anti-nidogen-1 (Figure 4T), and anti-collagen IV (Figure 4U). As a control, Figure 4V indicate that anti-collagen IV antibody readily detect native collagen IV. In blots with wildtype brain extract, laminin and nidogen were both detected as a band at 120 kDa. The banding at 120 kDa indicated binding of laminin to α-DG and showed that nidogen-1 is in a complex with laminin-111. No such bands were detected in blots with LARGE-deficient brain extract. LARGE-deficient brain extract was chosen as a control because of complete abolishment of laminin binding by α-DG in this model. In contrast, collagen IV was not detected in the blots. These results show that laminin-111 and nidogen-1 are associated in Matrigel, but collagen IV is not part of a complex with either laminin-111 or nidogen-1. Indeed, laminin-111 and nidogen-1 can be co-immunoprecipitated (data not shown).

2.4. Assembly rate of BM on POMGnT1 knockout neural spheres was reduced

To evaluate whether POMGnT1 deficiency affected the rate of BM assembly, control and POMGnT1 knockout neural spheres were incubated with Matrigel. As incubation time increased from 15 minutes to 12 hours, laminin-111 (green fluorescence) and collagen IV (red fluorescence) immunofluorescence intensities on the surface of the control neurospheres (Figure 5A–F) increased. These results indicated that together with laminin-111 the aggregation of other ECM molecules on the surface of wildtype neural spheres increased over time. In contrast, laminin-111 and collagen IV immunofluorescence staining on POMGnT1 knockout neural spheres showed a reduced fluorescence for both laminin-111 and collagen IV at all time points (Figure 5A′–F′). The overall fluorescence intensity measurements revealed that both laminin-111 and collagen IV bound significantly less on POMGnT1 knockout neural spheres than on wildtype spheres (Figure 5G and H). Further, the average size (Figure 5I) and intensity (Figure 5J) of laminin immunofluorescence of individual aggregates deposited on POMGnT1 knockout neural spheres were smaller and reduced at all time points. We calculated the maximal fluorescence intensity, time to reach 50% maximal intensity, and initial rate of fluorescence increase by curve fitting for laminin-111 and collagen IV (Figure 5G and H). All three parameters were significantly reduced in POMGnT1 knockout neural stem cells (Table I). The initial rate of laminin-111 immunofluorescence increase for wildtype neural stem cells was 15.53 ± 1.982 Arbitrary Units/hour. In contrast, the initial rate for POMGnT1 knockout neural stem cells

was 5.832 ± 1.925 Arbitrary Units/hour (p = 0.024, F test). The initial rate of collagen IV immunofluorescence for wildtype neural stem cells was 13.19 ± 2.223 Arbitrary Units/hour. In contrast, the initial rate for POMGnT1 knockout neural stem cells was 5.646 ± 1.951 Arbitrary Units/hour (p = 0.058, F test). Similar results were obtained for nidogen-1 and perlecan (Supplementary Figure 4 and Table I). Together, these data show that the assembly rate of BM on the surface of POMGnT1 knockout neural spheres is reduced.

2.5. Selective reduction of laminin-111 and nidogen-1 in POMGnT1 knockout ILM

A reduced rate of ECM assembly in POMGnT1 knockout mice may have resulted in an altered BM protein composition. Therefore, we compared the relative levels of several key components of the ILM from control and POMGnT1 knockout mice (Hu et al., 2010). The ILM, instead of the pial basement membrane, was chosen because it has the same developmental origin as the pial basement membrane and it is disrupted at the same developmental stage as the pial basement membrane in POMGnT1 knockout mice (Hu *et al.*, 2010;Hu *et al.*, 2007). Furthermore, the ILM is largely devoid of vasculature while the pial surface is rich in vasculature. Sections from both POMGnT1 knockout and wildtype littermate controls were collected on the same slide and immunostained with antibodies against laminin-111 (Figure 6A and B), collagen IV (Figure 6E and F), nidogen-1 (Figure 6I and J), and perlecan (Figure 6M and N). Compared to wildtype, the fluorescence intensity of laminin-111 and nidogen-1 was reduced in POMGnT1 knockout ILM (Figure 6C and K, $p<0.01$, $n=6$). No significant changes were observed for collagen IV and perlecan (Figure 6G and O). As an internal control, the immunofluorescence intensities of laminin-111, nidogen-1, collagen IV and perlecan were also measured for the blood vessel BMs that are not affected by this mutation. No significant changes were observed for this BM (Figure 6D, H, L, and P). Further, we also carried out immunofluorescence staining of whole-mount retinas with antibodies to laminin-111 and collagen IV (Supplementary Figure 5). The immunofluorescence intensity of laminin-111 on the ILM was reduced in POMGnT1 knockout retina. Changes in collagen IV, however, were not statistically significant. These results suggest that laminin-111 and nidogen-1 were selectively reduced in POMGnT1 knockout ILMs.

To confirm the immunocytochemistry results, we carried out quantitative proteomics on isolated ILMs from wildtype and POMGnT1 knockout mice. Relative levels of BM proteins from two independent experiments are listed in Table II. Laminin α-1 and γ-1 chains, two subunits of laminin-111, were identified in both experiments and their relative levels were higher in the wildtype than POMGnT1 knockout mice. Nidogen-1 was also identified in both experiments, and its level was higher in the wildtype than POMGnT1 knockout mice as well. Conversely, the levels of α-1 and α-2 chains of collagen IV and perlecan were lower in the wildtype than POMGnT1 knockout mice. These results indicate that there is a selective reduction in a subset of BM components in POMGnT1 knockout ILM that includes laminin-111 and nidogen-1.

2.6. Structural changes in POMGnT1 knockout ILM

Changes in the protein composition of the BM may result in structural changes. We therefore investigated the surface topography of POMGnT1 knockout ILM with atomic force microscopy. Figure 7A and B shows the color-coded surface topography of wildtype and POMGnT1 knockout ILMs. Darker color indicates lower height while brighter color indicates higher height. Regions with darker color were referred to as “valleys”. POMGnT1 knockout ILM exhibited an increased number of large “valleys” as compared to wildtype littermate controls. To quantify this effect, the size of “valleys” was measured. The distribution of large “valleys” was tilted to the POMGnT1 knockout ILM (Figure 7C, Yates Chi-Square analysis, $X^2=15.7$, $p<0.0001$). To analyze the trend of changes, the odds ratio of

the number of "valleys" was calculated for each bin. The natural logarithm of the odds ratio indicated a linear relationship, such that the bigger a "valley" is, the more likely it occurs in the POMGnT1 knockout ILM (Figure 7D, $p<0.0001$, Fisher's exact test). These results indicate structural changes in POMGnT1 knockout ILMs.

Additionally, a reduction in key components of BMs may also cause a reduction in BM thickness. We therefore measured the thickness of the ILM preparations as described previously (Candiello et al., 2007) from six POMGnT1 knockout and six wildtype ILMs. The wildtype ILM had a thickness of 82 ± 3.3 nm (mean ± SEM). However, the thickness of POMGnT1 knockout ILM was 53 ± 3.7 nm ($p<0.0001$, Student's t test), indicating a significantly reduced thickness (an example of AFM scanning is shown in Figure 7E). These results indicate that the thickness of the ILM in POMGnT1 knockout mice was thinner.

3. Discussion

A hallmark of dystroglycanopathies is the physical disruptions of the BM that lead to neuronal ectopia in the neocortex, the cerebellum, and the retina. The mechanisms of BM disruptions are poorly understood. In a previous report, we have shown that the ILM of POMGnT1 knockout and Large^{myd} mice were physically weakened (Hu et al., 2010). In this report, using POMGnT1 knockout neural stem cells as a model system, we found, that the rate of BM assembly in POMGnT1 knockout mice is impaired. POMGnT1 knockout mice exhibited reduced levels of laminin-111 and nidogen-1 in the ILM as well as an altered ILM surface structure. In addition, POMGnT1 knockout ILMs were significantly thinner than ILMs in wildtype. These results, together with our previous finding (Hu et al., 2010), showed that the BMs in POMGnT1 knockout mice are biomechanically weaker due to an impaired BM assembly.

α-DG plays a key role in assembly of the BM and brain specific knockout of DG results in disruption of the pial BM and causes neuronal ectopia (Henry and Campbell, 1998;Moore et al., 2002). Our data showed that α-DG targeting in radial glia and in neural stem cells was not affected in POMGnT1 knockout mice. This is consistent with the finding that an intact dystrophin-glycoprotein complex (DGC) is present in muscles from Large^{myd} mice (Han *et al.*, 2009a).

Our findings that POMGnT1 knockout neural stem cells exhibited reduced maximal binding and reduce size of laminin-111 aggregates are consistent with previous findings. Deletion of dystroglycan (Henry and Campbell, 1998;Montanaro et al., 1999) or β1 integrins (Colognato et al., 1999;Lohikangas et al., 2001;Montanaro et al., 1999) leads to significant reduction of laminin-111 binding on the cell surface. Further, laminin-111 fails to organize into more complex aggregates on the surface of dystroglycan or integrin β1 deficient cells (Henry et al., 2001;Tsiper and Yurchenco, 2002). However, whether DG is required for BM formation on embryonic bodies *in vitro* is still debated (Henry and Campbell 1998; Li et al., 2002). In addition, galactosylsulfatide on Schwann cells also facilitate laminin binding on the surface (Li and Yunchenco, 2005). In this study, we established an *in vitro* BM assembly model and used this model to measure the rate of BM assembly in control and knockout cells. Our results showed that POMGnT1 deficiency resulted in a significantly reduced rate of BM assembly. These effects are likely due to hypoglycosylation of α-DG since microarray experiments revealed no changes in expression of integrins (data not shown), and Western blot analysis revealed no changes in β-1 integrin as well (Supplementary Figure 6).

Expression of laminin γ1 is reduced in integrin-β1 null embryonic stem cells (Li, et al, 2002). Expression of laminin α1 mRNA is up-regulated but expression of laminin α2 mRNA is down-regulated in morpholino-mediated knock-down of fukutin and FKRP in zebrafish embryos (Lin *et al.*, 2011). Interestingly, the expression of laminin-111 in neural

stem cells is unchanged in POMGnT1 knockout neural stem cells (bands indicated by asterisk in Supplementary Figure 1C). *In vivo* expression of all four major components of BM is unchanged in the developing neocortex as well (Supplementary Figure 2). These differences suggest that the mechanisms of BM disruptions differ between POMGnT1 knockout and integrin β-1 knockout mice.

Recently, it was suggested that laminin deposition is altered within the cerebral cortex of FKRP knock-down mice (Ackroyd *et al.*, 2011). The laminin staining pattern in FKRP knock-down mice is similar to that observed for POMGnT1 knockout mice (Hu *et al.*, 2007). In POMGnT1 knockout mice, the altered laminin expression pattern in brain is caused by the meningeal cells that are displaced by neurons that overmigrated through the disrupted pial BM. Analysis of multiple developmental stages in POMGnT1 knockout mice reveals that overmigration of neurons through the disrupted pial basement membrane into the leptomeninges results in meningeal cells being ectopically located within the developing cortex (Hu *et al.*, 2007). Since meningeal cells produce laminin (Sievers *et al.*, 1994), and ectopic meningeal cells in the cortex maintain their laminin production, it creates the impression of an altered laminin expression in cortex. This appears to be at odds with the conclusion of the FKRP knock-down study that suggested an increased expression of laminin in the cortex of these mice. Indeed, when we analyzed the expression of laminin in the entire neocortical wall of POMGnT1 knockout mice, we saw no changes in expression as compared to wildtype controls. Thus, we feel that the FKRP knock-down cortices need to be re-examined for disruptions of the pial basement membrane, overmigration of neurons, and ectopia of meningeal fibroblasts to determine whether the abnormal laminin pattern in FKRP knock-down mice is contributed by ectopic location of meningeal cells.

The reduction of laminin-111 and nidogen-1 in POMGnT1 knockout ILM is likely caused by the reduced rate of BM assembly since synthesis and expression of these BM components were unchanged. While assembly of all four major components of the BM onto POMGnT1 knockout neural spheres was reduced *in vitro*, only laminin-111 and nidogen-1 were reduced significantly in POMGnT1 knockout ILM. The Matrigel assembly assay lasted only 24 hours with very little extracellular matrix, if any, assembled at the beginning of the assay. However, fully functional BM already existed prior to their disruptions *in vivo* in POMGnT1 knockout mouse model (Hu, et al, 2007). Therefore, the *in vitro* assembly model cannot fully mimic the assembly of a BM *in vivo*. Additionally, nidogen-1 is tightly associated with laminin-111 as a complex (Balasubramani *et al.*, 2010;Yurchenco and Schittny, 1990), providing an explanation that nidogen-1 be more directly affected by reduced laminin than other BM components. We were surprised that perlecan was not reduced *in vivo*. Perlecan has been reported to bind multiple receptors such as integrin beta 1 and 3 (Hayashi *et al.*, 1992) and DG (Talts *et al.*, 1999b), and connect laminin with collagen IV network (LeBleu *et al.*, 2007). Moreover, the binding between perlecan with DG is also dependent on the glycosylation of DG (Henry *et al.*, 2001). Lack of reduction in perlecan in ILM might be due to a compensatory mechanism *in vivo* by other receptors such as integrins that may be sufficient to allow normal perlecan assembly regardless of α-DG hypoglycosylation.

Different physical properties are associated with two other BMs: Bowman's membrane and Descemet's membrane of the human cornea (Last et al., 2009). The Young's modulus of Descemet's membrane is higher than for Bowman's membrane. Interestingly, the topography of Descemet's membrane exhibits smaller "valley" sizes in general when compared to that of Bowman's membrane, suggesting a relationship between the observed Young's modulus and structural features. In this study, the POMGnT1 knockout ILM exhibited significantly bigger "valleys", demonstrating a less tightly packed structure. We speculate that the loose structure is possibly due to reduced levels of laminin-111 and

nidogen-1. The structural change may also account for the reduced Young's modulus in POMGnT1 knockout ILM (Hu et al., 2010) and the reduced ILM thickness. The reduced thicknesses as well as reduced Young's modulus most likely account for a physically weakened BM in POMGnT1 knockout mice. Although the compromised BM appears normal under EM, they are broken under a physical stress. For instance, pial BM is broken around E13.5 in POMGnT1 knockout mice when the cortex is rapidly expanding (Hu *et al.*, 2007) and BM in skeletal muscle is disrupted after extensive excises in DG muscle-specific conditional knockout and LARGE^{myd} mice (Han *et al.*, 2009b).

It is of interest to note that not all BMs are affected in POMGnT1 knockout mice. No disruption is found in blood vessel BM in the brain (Hu *et al.*, 2007). It is not uncommon for genetic deficiencies to cause differential effects on the integrity of different BMs. For examples, Alport syndrome preferentially affects the glomerular BM of the kidney (Colville and Savige, 1997). Dystroglycanopathies preferentially affect the pial BM, ILM, and skeletal muscle BM. While laminin α2 deficiency causes skeletal muscle BM defects (Jimenez-Mallebrera *et al.*, 2005), the pial BM is not affected. Differential effects on various BMs are likely caused by heterogeneity in BM biochemical composition, differential expression of cellular receptors, and/or differences in mechanical strain exerted onto the BMs. Why POMGnT1 deficiency affects integrity of some but not other BMs will need to be investigated.

Based on the present data, we propose the following model regarding the mechanisms of BM disruptions in POMGnT1 knockout mice. First, diminished binding of ECM to the hypoglycosylated α-DG results in a reduced assembly rate of the BMs. Second, the reduced assembly leads to reduced incorporation of a subset of protein components in the newly assembled BM as the brain expands during development. Third, the protein deficiencies result in structural changes in the BM lattice, eventually leading to reduced physical strength due to a reduced stiffness and thickness. The reduced rate of assembly and defective physical strength of the BM make it vulnerable to mechanical stress exerted by rapidly expanding tissues during development, leading to disruptions. Since LARGE overexpression leads to functional hyperglycosylation in cells with mutations in other genes and rescues extracellular matrix binding activity of these cells (Barresi *et al.*, 2004;Zhang and Hu, 2012;Zhang *et al.*, 2011), future studies need to be directed at understanding whether LARGE glycosylation of α-DG and related proteins promotes BM assembly and whether such activities can be used to prevent disruptions of the BMs.

4. Experimental procedures

4.1. Animals and neural stem cell culture

Embryonic day 13.5 fetuses of POMGnT1 knockout mice (Liu et al., 2006) were used to generate neural stem cell cultures as described (Hu et al., 2011a). For timed pregnancy, 12:00 noon on the day plug was designated as embryonic day (E) 0.5. Genotyping of neural stem cells was carried out by PCR as described elsewhere (Liu et al., 2006). Neural stem cells were maintained as neural spheres. For the monolayer culture, neural stem cells were grown in eight well-chamber slides coated by 4 μg/ml fibronectin.

In utero electroporation of E13.5 fetuses with pCAG-DG-EGFP vector was performed as described previously (Olson et al., 2006). Fetuses were allowed to develop one more day after surgery and then were sacrificed and sectioned to observe GFP expression.

4.2. Antibodies and purified proteins

Antibodies were obtained as follows: Rabbit polyclonal anti-Nidogen-1 (1:300 dilution) from Abcam Inc. (Cambridge, MA); Rabbit anti-mouse collagen IV polyclonal antibody

(1:500 dilution) from Chemicon International, Inc.; Rabbit polyclonal anti-Laminin-111 and mouse monoclonal antibody against laminin-111 (1:500 dilution) from Sigma-Aldrich, Inc. (St. Louis, MI); Rat monoclonal antibody anti-perlecan Ab-1 (1:150 dilution) from Thermo Scientific (Fremont, CA); Mouse monoclonal IgM IIH6C4 (Ervasti and Campbell, 1993) (1:2000 dilution) from Millipore Corporation (Billerica, MA); Anti-β-DG (MANDAG2-7D11) from Developmental Studies Hybridoma Bank (University of Iowa, Department of Biology, Iowa City, IO); Mouse serum anti-nestin (1:10 dilution) was a gift from Dr. Russell T Matthews (SUNY Upstate Medical University, Syracuse, NY).

Purified proteins were obtained as follows: laminin-111 from Invitrogen, Inc. (Grand Island, NY); Recombinant human nidogen-1 from R&D Systems Inc. (Minneapolis, MN); Collagen IV from Trevigen Inc. (Gaithersburg, MD): and Matrigel from BD Biosciences (San Diego, CA).

4.3. Adenoviral vector

An adenoviral vector for EGFP tagged human POMGnT1 (Ad-POMGnT1-EGFP) was constructed at Vector Biolabs (Philadelphia, PA) on a fee-for-service basis.

4.4. Laminin-111, collagen IV, nidogen-1 and Matrigel assembly assay on cells

Neural stem cells were cultured as neural spheres in 100 mm suspended tissue-culture dishes. Neural spheres were incubated with laminin-111 (10 μg/ml), collagen IV (10 μg/ml), nidogen-1 (μg/ml), or Matrigel (20 μg/ml). The cells were then fixed with 4% paraformaldehyde and immunofluorescence stained with specific antibodies to observe bound protein.

For laminin-111 assembly assay on monolayer culture, neural stem cells were cultured in fibronectin-coated eight well-chamber slides and infected with Ad-POMGnT1 for 48 hours. Laminin-111 was then added into individual chamber. After incubation, the cells were fixed with 4% paraformaldehyde and immunofluorescence stained with anti-laminin-111 to observe bound laminin.

Immunofluorescence staining—For immunofluorescence staining of retinal sections, mice at postnatal day 3 were perfused with 4.0% paraformaldehyde. POMGnT1 knockout and wildtype eyes were dissected out and snap frozen in OCT media with 2-methylbutane/dry ice baths, cryostat-sectioned at 10 μm, and mounted on the same Superfrost plus slides (Fisher Scientific, Pittsburgh, PA, USA). The sections were fixed with 4% paraformaldehyde for 30 min and blocked for 1 hr with 3% BSA in 0.1 M phosphate buffer (PB). Immunofluorescence staining was carried out as previously described (Hu, 2000). Briefly, sections were incubated with primary antibodies diluted in 3% BSA overnight at 4 °C. After washing with PB, they were incubated with appropriate secondary antibodies conjugated with fluorescein isothiocyanate (FITC) or rodamine isothiocyanate (RITC) for 2 hours at room temperature. The sections were mounted with Vectashield® mounting medium (Vector Laboratories, Inc., Burlingame, CA) and covered with cover slips. Fluorescence was visualized with a Zeiss Axioskop upright fluorescence microscope equipped with a digital camera (Carl Zeiss Microimaging, Inc., Thornwood, NY).

For immunofluorescence staining of neural spheres, the fixed neural spheres were pelleted by centrifugation at 100 g for 2 min. After washing with PBS containing 0.1% BSA, 1 mM $CaCl_2$ and $MgCl_2$ three times, the spheres were immunofluorescence stained. To mount the neural spheres onto slides without compression, the spheres were embedded into 3% low-melting agarose and cut into 200 μm sections with a vibratome.

All figures involving fluorescence images were prepared with Photoshop 5.0 (Adobe Systems Incorporated, San Jose, CA). Brightness and/or contrast of micrographs in some figure panels were adjusted for clarity.

Quantification of immunofluorescence intensities—To quantify fluorescence levels of immunofluorescence staining of neural spheres, Zeiss LSM510 confocal microscope was used for image acquisition. Care was taken such that the images were not overexposed. Briefly, Range Indicator was selected to demonstrate a false color lookup table that shows saturated pixels in red (255) and underexposed pixels in blue (0). During image acquisition, strongest signals from wildtype after 12 hours incubation were used to adjust the parameters such that only a few red pixels were shown in Range Indicator table. Signals from cells not exposed to laminin-111 or Matrigel but immunofluorescence stained were used to set up background such that only a few blue pixels were displayed in Range Indicator table. Image analysis and quantification were performed using ImageJ software (v. 1.42I, compliments of NIH). For overall fluorescence intensity measurement, specific areas were circled and directly measured. The fluorescent intensity per unit area was used in comparison between different samples. For monolayer cultures, the overall fluorescence intensity was normalized to total cell number in the area of interest.

In order to study individual aggregates on neural spheres, particle analysis function in ImageJ was used to measure intensity, area, particle numbers, and total spherical area. The pixel value exacted from background was set as threshold to segment the object from the background.

4.5. Electron microscopy

Neural stem cells were cultured on fibronectin-coated Thermanox™ coverslips (Rochester, NY). For Matrigel assay, 20 μg/ml Matrigel was added to the culture medium containing 1% BSA and 1 mM $CaCl_2$ and $MgCl_2$. After 7 days of incubation, cells were washed with TBS buffer and fixed with 3.7% glutaraldehyde. The cells were postfixed in 1% osmium tetroxide, stained with 1% uranyl acetate, and embedded in Poly/Bed 812 resin (Polysciences, Warrington, PA). Ultra-thin sections were cut and stained with 2% uranyl acetate and Reynold's lead citrate (Polysciences). Electron microscopic micrographs were collected with a Tecnai BT12 transmission electron microscope (FEI, Salem, MA).

4.6. Modeling of extracellular matrix assembly and calculation of initial assembly rates

To determine the assembly rate of ECM molecules on neural stem cell cultures, normalized immunofluorescence intensity was plotted as a function of incubation time. Non-linear curves were fitted to the plots based on the following equation by using GraphPad Prism 5 (La Jolla, CA):

$$Y=B_{max} \cdot X/(T_{1/2}+X)$$

Where Y = mean fluorescence intensity per μm^2; X = incubation time (hour); $T_{1/2}$ = time to reach 50% maximal intensity; and B_{max} = maximal fluorescence intensity.

$$\text{The slope of the curve } (V)=Y/X=B_{max}/(T_{1/2}+X)$$

When X approaches zero, the initial slope of the curve ($V_{initial}$) = $B_{max}/T_{1/2}$ and is computed by GraphPad Prism 5. Statistical analysis of the calculated initial rate was by F test with GraphPad Prism 5.

4.7. Western blot, laminin, and Matrigel overlay assays

Cells were washed three times with ice-cold HBSS and lysed with pre-chilled cell lysis buffer (50 mM Tris-HCl, pH7.4, 150 mM NaCl, and 1% Triton X-100) containing proteinase inhibitor cocktail (Roche). The lysates were centrifuged at 16,000 g at 4°C for twenty minutes and supernatant was collected.

For enrichment of glycoproteins by wheat germ agglutinin (WGA)-agarose, 3 mg of proteins of the total lysate was mixed with 50 μl WGA-agarose (EY Laboratories, San Mateo, CA). After binding for 16 hrs, the gel was precipitated and washed three times with cold lysis buffer. Bound glycoproteins were eluted by SDS-PAGE gel loading buffer and separated on SDS-PAGE and electrotransferred onto polyvinylidene fluoride (PVDF) membranes.

For Western blot with IIH6C-4 and anti-β-DG antibodies, standard Western blot procedures were carried out. Briefly, the PVDF membrane was incubated with 3% BSA in TBST (50 mM Tris, pH7.4, 150 mM NaCl, 0.05% Tween-20) for one hr to block non-specific binding. The membranes were incubated with the primary antibodies in TBST containing 3% BSA overnight. After washing three times with TBST, the membranes were incubated with goat anti-mouse IgM or IgG conjugated with horseradish peroxidase (1:3000) for 45 min. After extensive washing with TBST, the signal was visualized with SuperSignal west pico chemiluminescence substrate (Thermo Scientific, Rockford, IL).

For laminin/Matrigel-overlay assay, the PVDF membrane was incubated with Tris-buffered saline (TBS, 50 mM Tris, pH7.4, 150 mM NaCl) containing 3% BSA, 1 mM $CaCl_2$, and 1 mM $MgCl_2$ for an hr to block nonspecific binding. The membrane was then incubated with 1.25 μg/ml laminin-111 (Invitrogen) or 2.5 μg/ml Matrigel in TBST containing 1mM $CaCl_2$ and 1 mM $MgCl_2$ overnight at 4 °C. After washing, detection of bound laminin-111, nidogen-1, or collagen IV was done by standard Western blot procedures in buffers containing 1 mM $CaCl_2$ and 1 mM $MgCl_2$.

Biotinylation—Neural stem cells were cultured in fibronectin-coated 100 mm dishes. After cells reach 95% confluence, they were rinsed by ice-cold PBS three times and incubated with 2 ml ECS (135 mM NaCl, 3 mM KCl, 2 mM $CaCl_2$, 2 mM $MgCl_2$, 20 mM glucose, 20 mM HEPES, pH 7.4) solution containing EZ-Link Sulfo-NHS-Biotin (Pierce) for 30 minutes at 4 °C. After biotinylation, Cells were quenched with glycine buffer twice and lysate was prepared as above. 1 mg total lysates from WT and POMGnT1 Knockout was immunoabsorbed by avidin-conjugated beads (Sigma, MO).

4.8. Atomic Force Microscopic analysis of the ILM

Flat-mount ILM was prepared as described before (Candiello *et al.*, 2007;Hu *et al.*, 2010). Briefly, retinas from P3 mice were spread onto nitrocellulose membrane (Millipore, Bedford, MA, USA) and placed onto poly-D-lysine-coated slides, vitreous surface down and covered with a coverslip for 5 minutes. The nitrocellulose membrane along with the retina was removed and the ILMs were washed several times with 2% Triton-X-100 in PBS for thirty minutes. For thickness measurement, the ILM were artificially scratched with a pipette tip. The height profile was recorded as a probe moves along the scratched edge to the flat segment of ILM. The thickness was measured from 6 pairs of wildtype and POMGnT1 knockout ILM as described (Candiello et al., 2007). For each ILM, eight measurements were performed in the randomly selected area. Student's t test was performed.

Surface topography was analyzed at the Nanoimaging Core Facility in University of Nebraska Medical Center. Quantification of number and size of "valleys" on scanning atomic force microscopic images was performed in a double-blind manner. Each image was

divided into sixteen small squares and numbered. Six squares were randomly chosen for each image. All “valleys” in the selected squares were circled and the areas were measured by Image J. The areas of the “valleys” were then sorted into different size groups. Chi-square analysis with Yates’ correction was performed to evaluate the difference between wildtype and POMGnT1 knockout ILMs.

4.9. Quantitative proteomics of the ILM

ILM for proteomic analysis was prepared as described previously (Balasubramani et al., 2010). Briefly, retinas were incubated in 2% Triton-X-100 for 2 hrs at room temperature to solubilize cellular components. The insoluble ILM was collected, transferred with a pipette tip to a new tube containing 2% Triton-X-100 for another 2 hrs at 4°C, and repeated three times. The ILM was pelleted by centrifugation at 3,000 g for 2 min and digested with trypsin. The resulting peptide mixtures were analyzed by LC-MS for quantitative analysis as described (Reidel et al., 2011;Soderblom, 2011). The levels of identified extracellular matrix proteins were normalized in the wildtype and POMGnT1 knockout ILMs separately. Relative abundance of individual proteins was then compared between POMGnT1 knockout and wildtype ILMs.

Supplementary Material

Refer to Web version on PubMed Central for supplementary material.

Acknowledgments

We thank Drs. Brian Howell, Eric Olson, and Russell Mathews for helpful discussions during the project. β-DG antibody was obtained from the Developmental Studies Hybridoma Bank at the University of Iowa. AFM scanning imaging was carried out at the Nanoimaging Core Facility in University of Nebraska Medical Center. We thank the Duke University School of Medicine for the use of the Duke Proteomics Core Facility, which provided label-free quantitative proteomic analysis service. This work was supported by National Institutes of Health grants HD060458 and NS066582 (to H.H) and the National Natural Science Foundation of China grant 30870867 (to Y.Y).

References

Ackroyd MR, Whitmore C, Prior S, Kaluarachchi M, Nikolic M, Mayer U, Muntoni F, Brown SC. Fukutin-related protein alters the deposition of laminin in the eye and brain. J Neurosci. 2011; 31:12927–12935. [PubMed: 21900571]

Balasubramani M, Schreiber EM, Candiello J, Balasubramani GK, Kurtz J, Halfter W. Molecular interactions in the retinal basement membrane system: a proteomic approach. Matrix Biol. 2010; 29:471–483. [PubMed: 20403434]

Barresi R, et al. LARGE can functionally bypass alpha-dystroglycan glycosylation defects in distinct congenital muscular dystrophies. Nat Med. 2004; 10:696–703. [PubMed: 15184894]

Beltran-Valero de BD, et al. Mutations in the O-mannosyltransferase gene POMT1 give rise to the severe neuronal migration disorder Walker-Warburg syndrome. Am J Hum Genet. 2002; 71:1033–1043. [PubMed: 12369018]

Beltran-Valero de BD, et al. Mutations in the FKRP gene can cause muscle-eye-brain disease and Walker-Warburg syndrome. J Med Genet. 2004; 41:e61. [PubMed: 15121789]

Brockington M, et al. Mutations in the fukutin-related protein gene (FKRP) identify limb girdle muscular dystrophy 2I as a milder allelic variant of congenital muscular dystrophy MDC1C. Hum Mol Genet. 2001; 10:2851–2859. [PubMed: 11741828]

Candiello J, Balasubramani M, Schreiber EM, Cole GJ, Mayer U, Halfter W, Lin H. Biomechanical properties of native basement membranes. FEBS J. 2007; 274:2897–2908. [PubMed: 17488283]

Colognato H, Winkelmann DA, Yurchenco PD. Laminin polymerization induces a receptor-cytoskeleton network. J Cell Biol. 1999; 145:619–631. [PubMed: 10225961]

Colville DJ, Savige J. Alport syndrome. A review of the ocular manifestations. Ophthalmic Genet. 1997; 18:161–173. [PubMed: 9457747]

Costell M, Gustafsson E, Aszodi A, Morgelin M, Bloch W, Hunziker E, Addicks K, Timpl R, Fassler R. Perlecan maintains the integrity of cartilage and some basement membranes. J Cell Biol. 1999; 147:1109–1122. [PubMed: 10579729]

Currier SC, et al. Mutations in POMT1 are found in a minority of patients with Walker-Warburg syndrome. Am J Med Genet A. 2005; 133:53–57. [PubMed: 15637732]

de Bernabe DB, et al. A homozygous nonsense mutation in the fukutin gene causes a Walker-Warburg syndrome phenotype. J Med Genet. 2003; 40:845–848. [PubMed: 14627679]

Ervasti JM, Campbell KP. A role for the dystrophin-glycoprotein complex as a transmembrane linker between laminin and actin. J Cell Biol. 1993; 122:809–823. [PubMed: 8349731]

Gee SH, Blacher RW, Douville PJ, Provost PR, Yurchenco PD, Carbonetto S. Laminin-binding protein 120 from brain is closely related to the dystrophin-associated glycoprotein, dystroglycan, and binds with high affinity to the major heparin binding domain of laminin. J Biol Chem. 1993; 268:14972–14980. [PubMed: 8325873]

Gee SH, Montanaro F, Lindenbaum MH, Carbonetto S. Dystroglycan-alpha, a dystrophin-associated glycoprotein, is a functional agrin receptor. Cell. 1994; 77:675–686. [PubMed: 8205617]

Grewal PK, Holzfeind PJ, Bittner RE, Hewitt JE. Mutant glycosyltransferase and altered glycosylation of alpha-dystroglycan in the myodystrophy mouse. Nat Genet. 2001; 28:151–154. [PubMed: 11381262]

Han R, et al. Basal lamina strengthens cell membrane integrity via the laminin G domain-binding motif of alpha-dystroglycan. Proc Natl Acad Sci U S A. 2009a; 106:12573–12579. [PubMed: 19633189]

Han R, et al. Basal lamina strengthens cell membrane integrity via the laminin G domain-binding motif of alpha-dystroglycan. Proc Natl Acad Sci U S A. 2009b; 106:12573–12579. [PubMed: 19633189]

Hayashi K, Madri JA, Yurchenco PD. Endothelial cells interact with the core protein of basement membrane perlecan through beta 1 and beta 3 integrins: an adhesion modulated by glycosaminoglycan. J Cell Biol. 1992; 119:945–959. [PubMed: 1385448]

Henry MD, Campbell KP. A role for dystroglycan in basement membrane assembly. Cell. 1998; 95:859–870. [PubMed: 9865703]

Henry MD, Satz JS, Brakebusch C, Costell M, Gustafsson E, Fassler R, Campbell KP. Distinct roles for dystroglycan, beta1 integrin and perlecan in cell surface laminin organization. J Cell Sci. 2001; 114:1137–1144. [PubMed: 11228157]

Hu H. Polysialic acid regulates chain formation by migrating olfactory interneuron precursors. J Neurosci Res. 2000; 61:480–492. [PubMed: 10956417]

Hu H, Candiello J, Zhang P, Ball SL, Cameron DA, Halfter W. Retinal ectopias and mechanically weakened basement membrane in a mouse model of muscle-eye-brain (MEB) disease congenital muscular dystrophy. Mol Vis. 2010; 16:1415–1428. [PubMed: 20680099]

Hu H, Li J, Gagen CS, Gray NW, Zhang Z, Qi Y, Zhang P. Conditional knockout of protein O-mannosyltransferase 2 reveals tissue specific roles of O-mannosyl glycosylation in brain development. J Comp Neurol. 2011a; 519:1320–1337. [PubMed: 21452199]

Hu H, Li J, Zhang Z, Yu M. Pikachurin interaction with dystroglycan is diminished by defective O-mannosyl glycosylation in congenital muscular dystrophy models and rescued by LARGE overexpression. Neuros Lett. 2011b; 489:10–15.

Hu H, Yang Y, Eade A, Xiong Y, Qi Y. Breaches of the Pial Basement Membrane and Disappearance of the Glia Limitans during Development Underlie the Cortical Lamination Defect in the Mouse Model of Muscle-eye-brain Disease. J Comp Neurol. 2007; 501:168–183. [PubMed: 17206611]

Inamori K, Yoshida-Moriguchi T, Hara Y, Anderson ME, Yu L, Campbell KP. Dystroglycan function requires xylosyl- and glucuronyltransferase activities of LARGE. Science. 2012; 335:93–96. [PubMed: 22223806]

Jimenez-Mallebrera C, Brown SC, Sewry CA, Muntoni F. Congenital muscular dystrophy: molecular and cellular aspects. Cell Mol Life Sci. 2005; 62:809–823. [PubMed: 15868406]

Kanagawa M, Omori Y, Sato S, Kobayashi K, Miyagoe-Suzuki Y, Takeda S, Endo T, Furukawa T, Toda T. Post-translational maturation of dystroglycan is necessary for pikachurin binding and ribbon synaptic localization. J Biol Chem. 2010

Kano H, et al. Deficiency of alpha-dystroglycan in muscle-eye-brain disease. Biochem Biophys Res Commun. 2002; 291:1283–1286. [PubMed: 11883957]

Kim DS, et al. POMT1 mutation results in defective glycosylation and loss of laminin-binding activity in alpha-DG. Neurology. 2004; 62:1009–1011. [PubMed: 15037715]

Kobayashi K, et al. An ancient retrotransposal insertion causes Fukuyama-type congenital muscular dystrophy. Nature. 1998; 394:388–392. [PubMed: 9690476]

Labelle-Dumais C, et al. COL4A1 Mutations Cause Ocular Dysgenesis, Neuronal Localization Defects, and Myopathy in Mice and Walker-Warburg Syndrome in Humans. PLoS Genet. 2011; 7:e1002062. [PubMed: 21625620]

Last JA, Liliensiek SJ, Nealey PF, Murphy CJ. Determining the mechanical properties of human corneal basement membranes with atomic force microscopy. J Struct Biol. 2009; 167:19–24. [PubMed: 19341800]

LeBleu VS, Macdonald B, Kalluri R. Structure and function of basement membranes. Exp Biol Med (Maywood). 2007; 232:1121–1129. [PubMed: 17895520]

Lee Y, Kameya S, Cox GA, Hsu J, Hicks W, Maddatu TP, Smith RS, Naggert JK, Peachey NS, Nishina PM. Ocular abnormalities in Large(myd) and Large(vls) mice, spontaneous models for muscle, eye, and brain diseases. Mol Cell Neurosci. 2005; 30:160–172. [PubMed: 16111892]

Levi S, Grady RM, Henry MD, Campbell KP, Sanes JR, Craig AM. Dystroglycan is selectively associated with inhibitory GABAergic synapses but is dispensable for their differentiation. J Neurosci. 2002; 22:4274–4285. [PubMed: 12040032]

Li J, Yu M, Feng G, Hu H, Li X. Breaches of the pial basement membrane are associated with defective dentate gyrus development in mouse models of congenital muscular dystrophies. Neurosci Lett. 2011; 505:19–24. [PubMed: 21970971]

Li S, Edgar D, Fassler R, Wadsworth W, Yurchenco PD. The role of laminin in embryonic cell polarization and tissue organization. Dev Cell. 2003; 4:613–624. [PubMed: 12737798]

Li X, Zhang P, Yang Y, Xiong Y, Qi Y, Hu H. Differentiation and developmental origin of cerebellar granule neuron ectopia in POMGnT1 knockout mice. Neurosci. 2008; 152:391–406.

Lin YY, White RJ, Torelli S, Cirak S, Muntoni F, Stemple DL. Zebrafish Fukutin family proteins link the unfolded protein response with dystroglycanopathies. Hum Mol Genet. 2011; 20:1763–1775. [PubMed: 21317159]

Liu J, Ball SL, Yang Y, Mei P, Zhang L, Shi H, Kaminski HJ, Lemmon VP, Hu H. A genetic model for muscle-eye-brain disease in mice lacking protein O-mannose 1, 2-N-acetylglucosaminyltransferase (POMGnT1). Mech Dev. 2006; 123:228–240. [PubMed: 16458488]

Lohikangas L, Gullberg D, Johansson S. Assembly of laminin polymers is dependent on beta1-integrins. Exp Cell Res. 2001; 265:135–144. [PubMed: 11281651]

Longman C, et al. Mutations in the human LARGE gene cause MDC1D, a novel form of congenital muscular dystrophy with severe mental retardation and abnormal glycosylation of alpha-dystroglycan. Hum Mol Genet. 2003; 12:2853–2861. [PubMed: 12966029]

Manya H, Chiba A, Yoshida A, Wang X, Chiba Y, Jigami Y, Margolis RU, Endo T. Demonstration of mammalian protein O-mannosyltransferase activity: coexpression of POMT1 and POMT2 required for enzymatic activity. Proc Natl Acad Sci U S A. 2004; 101:500–505. [PubMed: 14699049]

Michele DE, et al. Post-translational disruption of dystroglycan-ligand interactions in congenital muscular dystrophies. Nature. 2002; 418:417–422. [PubMed: 12140558]

Montanaro F, Lindenbaum M, Carbonetto S. alpha-Dystroglycan is a laminin receptor involved in extracellular matrix assembly on myotubes and muscle cell viability. J Cell Biol. 1999; 145:1325–1340. [PubMed: 10366602]

Moore SA, et al. Deletion of brain dystroglycan recapitulates aspects of congenital muscular dystrophy. Nature. 2002; 418:422–425. [PubMed: 12140559]

Olson EC, Kim S, Walsh CA. Impaired neuronal positioning and dendritogenesis in the neocortex after cell-autonomous Dab1 suppression. J Neurosci. 2006; 26:1767–1775. [PubMed: 16467525]

Peng HB, Ali AA, Daggett DF, Rauvala H, Hassell JR, Smalheiser NR. The relationship between perlecan and dystroglycan and its implication in the formation of the neuromuscular junction. Cell Adhes Commun. 1998; 5:475–489. [PubMed: 9791728]

Reidel B, Thompson JW, Farsiu S, Moseley MA, Skiba NP, Arshavsky VY. Proteomic profiling of a layered tissue reveals unique glycolytic specializations of photoreceptor cells. Mol Cell Proteomics. 2011; 10:M110. [PubMed: 21173383]

Roscioli T, et al. Mutations in ISPD cause Walker-Warburg syndrome and defective glycosylation of alpha-dystroglycan. Nat Genet. 2012; 44:581–585. [PubMed: 22522421]

Satz JS, Barresi R, Durbeej M, Willer T, Turner A, Moore SA, Campbell KP. Brain and eye malformations resembling Walker-Warburg syndrome are recapitulated in mice by dystroglycan deletion in the epiblast. J Neurosci. 2008; 28:10567–10575. [PubMed: 18923033]

Sievers J, Pehlemann FW, Gude S, Berry M. Meningeal cells organize the superficial glia limitans of the cerebellum and produce components of both the interstitial matrix and the basement membrane. J Neurocytol. 1994; 23:135–149. [PubMed: 8195812]

Smalheiser NR, Kim E. Purification of cranin, a laminin binding membrane protein. Identity with dystroglycan and reassessment of its carbohydrate moieties. J Biol Chem. 1995; 270:15425–15433. [PubMed: 7797531]

Soderblom EJ. Quantitative label-free phosphoproteomics strategy for multifaceted experimental designs. 2011

Sugita S, Saito F, Tang J, Satz J, Campbell K, Sudhof TC. A stoichiometric complex of neurexins and dystroglycan in brain. J Cell Biol. 2001; 154:435–445. [PubMed: 11470830]

Takeda S, et al. Fukutin is required for maintenance of muscle integrity, cortical histiogenesis and normal eye development. Hum Mol Genet. 2003; 12:1449–1459. [PubMed: 12783852]

Talts JF, Andac Z, Gohring W, Brancaccio A, Timpl R. Binding of the G domains of laminin alpha1 and alpha2 chains and perlecan to heparin, sulfatides, alpha-dystroglycan and several extracellular matrix proteins. EMBO J. 1999a; 18:863–870. [PubMed: 10022829]

Talts JF, Andac Z, Gohring W, Brancaccio A, Timpl R. Binding of the G domains of laminin alpha1 and alpha2 chains and perlecan to heparin, sulfatides, alpha-dystroglycan and several extracellular matrix proteins. EMBO J. 1999b; 18:863–870. [PubMed: 10022829]

Tsiper MV, Yurchenco PD. Laminin assembles into separate basement membrane and fibrillar matrices in Schwann cells. J Cell Sci. 2002; 115:1005–1015. [PubMed: 11870219]

van Reeuwijk J, et al. POMT2 mutations cause alpha-dystroglycan hypoglycosylation and Walker-Warburg syndrome. J Med Genet. 2005; 42:907–912. [PubMed: 15894594]

Willer T, et al. ISPD loss-of-function mutations disrupt dystroglycan O-mannosylation and cause Walker-Warburg syndrome. Nat Genet. 2012; 44:575–580. [PubMed: 22522420]

Willer T, et al. Targeted disruption of the Walker-Warburg syndrome gene Pomt1 in mouse results in embryonic lethality. Proc Natl Acad Sci U S A. 2004; 101:14126–14131. [PubMed: 15383666]

Williamson RA, Henry MD, Daniels KJ, Hrstka RF, Lee JC, Sunada Y, Ibraghimov-Beskrovnaya O, Campbell KP. Dystroglycan is essential for early embryonic development: disruption of Reichert's membrane in Dag1-null mice. Hum Mol Genet. 1997; 6:831–841. [PubMed: 9175728]

Yamada H, Denzer AJ, Hori H, Tanaka T, Anderson LV, Fujita S, Fukuta-Ohi H, Shimizu T, Ruegg MA, Matsumura K. Dystroglycan is a dual receptor for agrin and laminin-2 in Schwann cell membrane. J Biol Chem. 1996; 271:23418–23423. [PubMed: 8798547]

Yamada H, Shimizu T, Tanaka T, Campbell KP, Matsumura K. Dystroglycan is a binding protein of laminin and merosin in peripheral nerve. FEBS Lett. 1994; 352:49–53. [PubMed: 7925941]

Yamamoto T, Toyoda C, Kobayashi M, Kondo E, Saito K, Osawa M. Pial-glial barrier abnormalities in fetuses with Fukuyama congenital muscular dystrophy. Brain Dev. 1997; 19:35–42. [PubMed: 9071488]

Yoshida A, et al. Muscular dystrophy and neuronal migration disorder caused by mutations in a glycosyltransferase, POMGnT1. Dev Cell. 2001; 1:717–724. [PubMed: 11709191]

Yurchenco PD, Schittny JC. Molecular architecture of basement membranes. FASEB J. 1990; 4:1577–1590. [PubMed: 2180767]

Yurchenco PD, Wadsworth WG. Assembly and tissue functions of early embryonic laminins and netrins. Curr Opin Cell Biol. 2004; 16:572–579. [PubMed: 15363809]

Zhang P, Hu H. Differential glycosylation of á-dystroglycan and proteins other than á-dystroglycan by LARGE. Glycobiol. 2012; 22:235–247.

Zhang Z, Zhang P, Hu H. LARGE expression augments the glycosylation of glycoproteins in addition to α-dystroglycan conferring laminin binding. PLoS ONE. 2011; 6:e19080. [PubMed: 21533062]

Highlights

- The rate of extracellular matrix assembly on POMGnT1 knockout spheres is significantly reduced.
- Laminin-111 and nidogen-1 are reduced in the POMGnT1 knockout mice inner limiting membrane.
- POMGnT1 knockout inner limiting membrane is thinner with an altered surface inner limiting membrane topography.

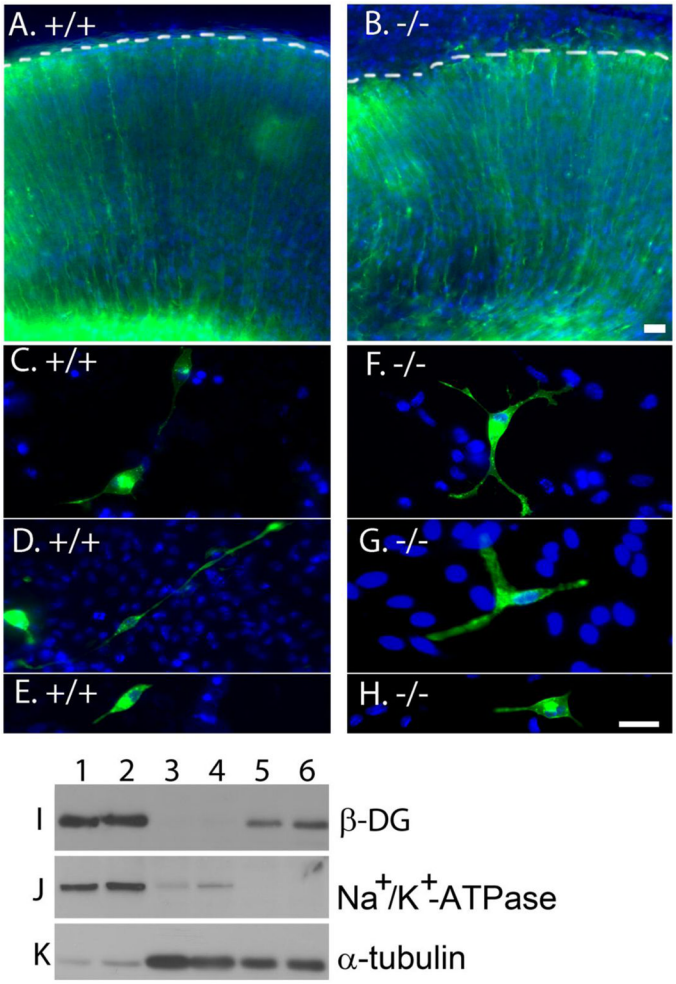

Figure 1. POMGnT1 knockout did not affect cellular distribution of dystroglycan

Distribution of EGFP-tagged dystroglycan was analyzed in the neocortical wall (A and B) and neural stem cells (C–H) after transfection by plasmid pCAG-DG-EGFP. (A) Wildtype neocortical wall. (B) POMGnT1 knockout neocortical wall. (C, D, and E) Wildtype neural stem cells. (F, G, and H) POMGnT1 knockout neural stem cells. Distribution of GFP fluorescence was indistinguishable between wildtype and POMGnT1 knockout. (I–K) Plasma membrane localization of dystroglycan was not changed in POMGnT1 knockout neural stem cells. Lanes 1 and 2: Biotinylated cell surface protein of wildtype (lane 1) and POMGnT1 knockout (lane 2) neural stem cells. Lanes 3 and 4: Total lysate protein of wildtype (lane 3) and POMGnT1 knockout neural stem cells. Lanes 5 and 6: Glycoprotein isolated by WGA-agarose from wildtype (5) and POMGnT1 knockout (6) neural stem cells. Note β-DG was equally detected in biotinylated cell surface protein fraction between the wildtype and POMGnT1 knockout neural stem cells. As controls, Western blotting for Na^+-K^+-ATPase and tubulin indicated high enrichment of plasma membrane proteins in biotinylated protein fraction. Scale bar in B: 2 μm for A and B. Scale bar in H: 2 μm for C–H.

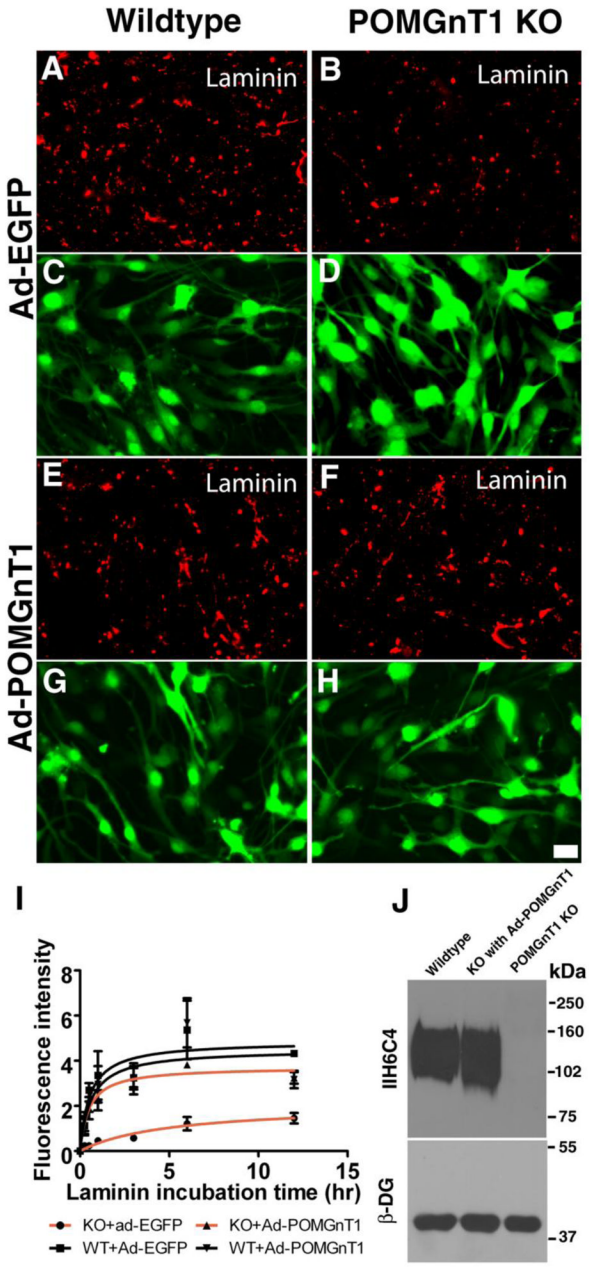

Figure 2. Laminin binding to POMGnT1 knockout neural stem cells was reduced

Neural stem cells were infected with Ad-EGFP or Ad-POMGnT1 for 48 hours. Laminin-111 was added to the culture medium. After 12 hours of incubation, bound laminin-111 was detected by immunofluorescence staining (A, B, E, and F). Green channel demonstrated a similar expression of adenovirus across all the samples (C, D, G, and H). (A and C) Wildtype infected with Ad-EGFP. (B and D) POMGnT1 knockout infected with Ad-EGFP. (E and G) Wildtype cells infected with Ad-POMGnT1. (F and H) POMGnT1 knockout cells infected with Ad-POMGnT1. Note that bound laminin-111 in POMGnT1 knockout neural stem cells was reduced (compare B with A). However, Ad-POMGnT1 infection restored laminin binding activity of POMGnT1 knockout cells (compare E with F). (I) Quantification of laminin immunofluorescence. (J) Western blot of glycoproteins isolated by WGA-agarose

with IIH6C4 and anti-β-DG. Abbreviations: kDa, kilodalton; KO, knockout. Scale bar in H: 2 μm.

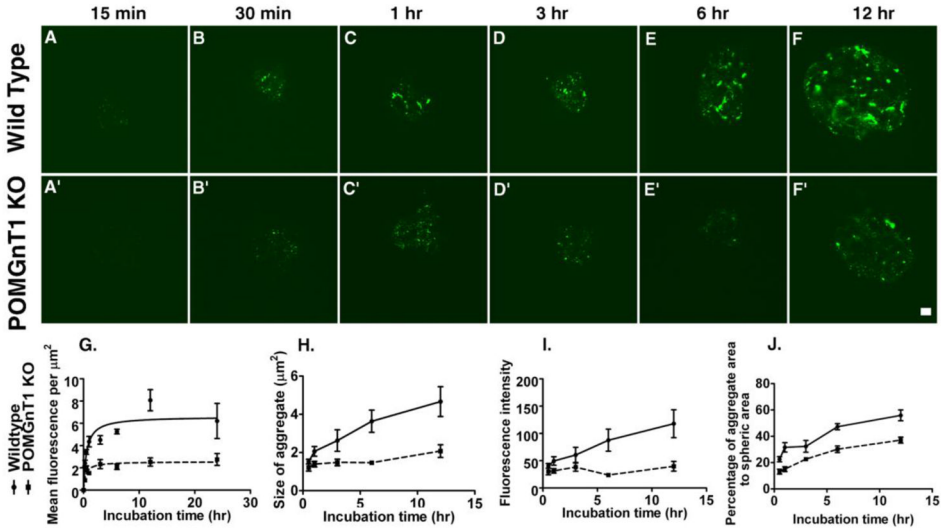

Figure 3. POMGnT1 deficiency resulted in a reduced rate of laminin accumulation on neural spheres

Neural spheres were incubated with laminin-111 for variable length of time and bound laminin-111 was detected by immunofluorescence staining. (A–F) Wildtype. (A′–F′) POMGnT1 knockout. (G) Fluorescence intensity per μm^2. (H) The average size of aggregates (μm^2). (I) Average fluorescence intensity per aggregate. (J) The percentage area of aggregates to the spheric surface area. Scale bar in F′, 10 μm.

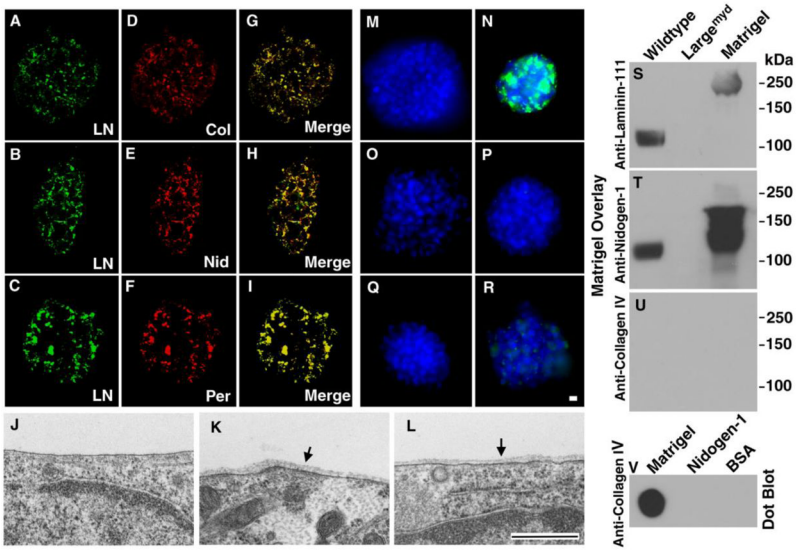

Figure 4. Co-localization of major BM components and formation of BM structure on neural stem cells after incubation with Matrigel

(A–I) Wildtype neural spheres were incubated with Matrigel for 24 hrs. Bound proteins including Laminin-111, collagen IV, nidogen-1, and perlecan were visualized by double immunofluorescence staining. Note co-localization of laminin-111 with collagen IV (A, D, and G), nidogen-1 (B, E, and H), and perlecan (C, F, and I).

(J–L) Wildtype neural stem cells were incubated with Matrigel (K and L) or without Matrigel (J) followed by electron microscopy. Incubation with Matrigel produced BM structures (arrows in K and L). BM was not observed in the absence of Matrigel incubation (J).

(M–R) Incubation of wildtype neural sphere with (N) or without (M) laminin-111, with (P) or without (O) collagen IV, and with (R) or without (Q) nidogen-1. Significant binding was observed for laminin-111 while residual binding was found for nidogen-1. No binding was observed for collagen IV.

(S–U) Matrigel gel overlay assay. Glycoproteins isolated by WGA-agarose from wildtype and Large^{myd} mouse brains were separated on SDS-PAGE and blotted onto PVDF membrane. After incubation with Matrigel, the membrane was detected with antibodies against laminin-111 (S), nidogen-1 (T), and collagen IV (U). Matrigel lane and Matrigel dot-blotted onto PVDF membrane (V) served as positive controls for antibody detection. Although collagen IV antibody did not detect denatured proteins, it detected native collagen IV (V). While laminin-111 and nidogen-1 were detected at 125 kDa location (expected location of glycosylated α-DG) in the wildtype, they were not detected in Large^{myd} sample. Abbreviations: KO, knockout; LN, laminin-111; Col, collagen IV; Nid, nidogen-1; Per, perlecan. Scale bar in R: 10 μm for A–I and M–R. Scale bar in L: 500 nm for J–L.

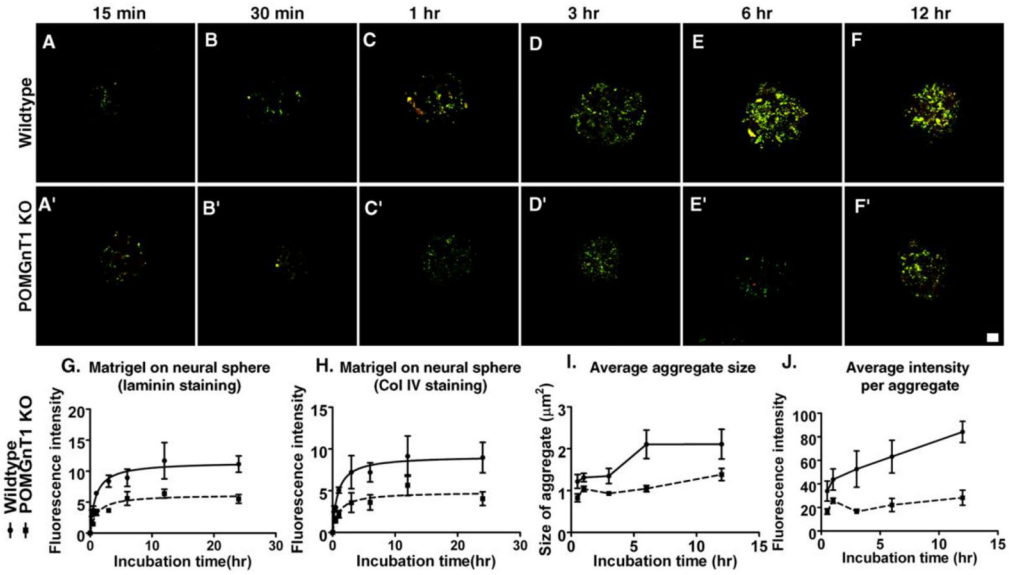

Figure 5. POMGnT1 knockout neural sphere exhibited a reduced rate of accumulation of BM components

Neural spheres were incubated with Matrigel for variable times and bound laminin-111 and collagen IV were visualized by immunofluorescence staining. (A–F) Wildtype. (A′-F′) POMGnT1 knockout. (G) Mean laminin-111 fluorescent intensity per μm^2. (H) Mean collagen IV fluorescence intensity per μm^2. (I) Average size of aggregates. (J) Average fluorescence intensity of aggregates. Scale bar in F′: 10 μm.

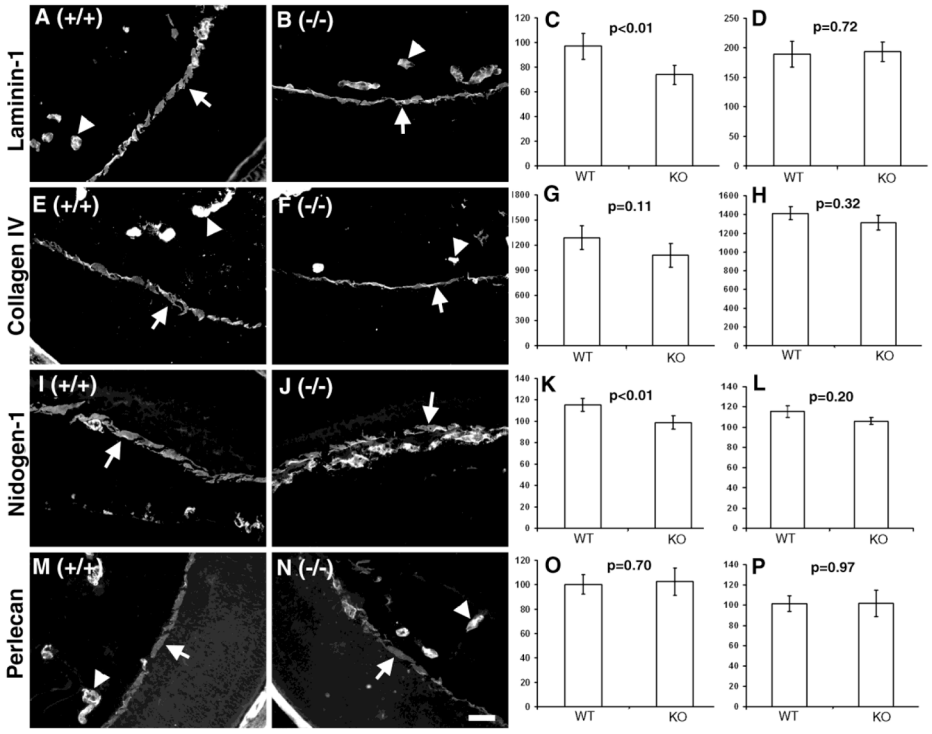

Figure 6. Laminin-111 and nidogen-1 were reduced in POMGnT1 knockout ILM

Eye sections of wildtype (A, E, I, and M) and POMGnT1 knockout mice (B, F, J, and N) were stained with antibodies against laminin-111 (A and B), collagen IV (E and F), nidogen-1 (I and J), and perlecan (M and N). The fluorescent intensity per μm^2 area was measured and quantified for ILM (C, G, K, and O) and blood vessels (D, H, L, and P). Note that laminin-111 and nidogen-1 were significantly reduced in POMgnT1 knockout ILM when compared to the wildtype. Arrows: ILM. Arrowheads: Blood vessels. Scale bar in N: 2 μm.

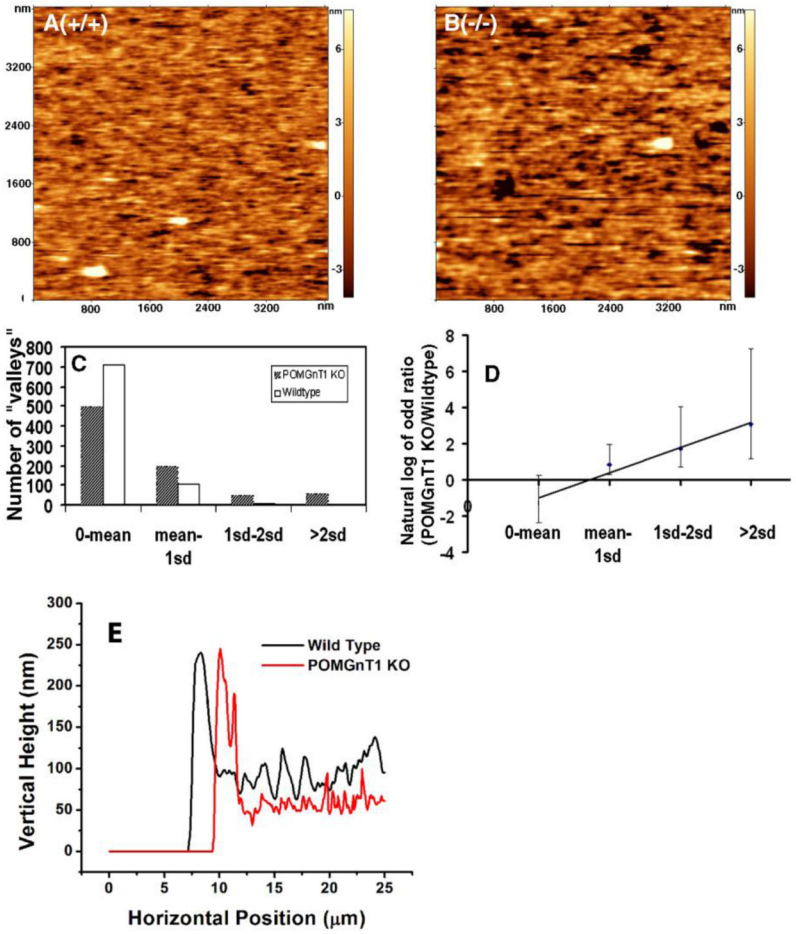

Figure 7. POMGnT1 knockout resulted in structural changes in ILM

The topographical feature of ILM was scanned using atomic force microscope. (A) Wildtype. (B) POMGnT1 knockout. (C) Histogram of “valleys” according to different bin sizes (o-Mean, Mean to 1 standard deviation (sd), 1 sd to 2 sd, bigger than 2 sd). (D) Odd ratio of POMGnT1 knockout versus the wildtype. Data presented are Mean ± standard error. (E) AFM thickness scanning. Abbreviations: KO, knockout; sd, standard deviation.

Table I

Initial assembly rate ($V_{initial}$) of ECM molecules on POMGnT1 KO neural stem cell cultures is reduced.

Cell lines	B_{max}	$T_{1/2}$	$V_{initial}$ (Mean ± SEM)	p value
laminin-111 overlay on monolayer cultures (Figure 2I)				
Wildtype + Ad-GFP	4.853	0.545	5.605 ± 0.896	
POMGnT1 KO+Ad-GFP	2.073	5.046	0.859 ± 0.214	<0.001
Wildtype + Ad-POMGnT1	4.496	0.619	5.631 ± 0.672	
POMGnT1 KO +Ad-POMGnT1	3.758	0.552	6.291 ± 0.428	0.442
Laminin-111 overlay on neural sphere cultures (Figure 3G)				
Wildtype	6.606	0.532	14.76 ± 1.772	
POMGnT1 KO	2.552	0.367	5.124 ± 0.926	0.002
Matrigel overlay (laminin-111 and collagen IV double staining) (Figure 5G and H)				
Wildtype (laminin-111)	11.47	0.895	15.53 ± 1.982	
POMGnT1 KO (laminin-111)	6.219	1.098	5.832 ± 1.925	0.024
Wildtype (collagen IV)	9.156	0.830	13.19 ± 2.223	
POMGnT1 KO (collagen IV)	4.840	1.015	5.646 ± 1.951	0.058
Matrigel overlay (laminin-111 and perlecan double staining) (Supplementary Figure 4F and G)				
Wildtype (laminin-111)	9.050	0.690	12.28 ± 0.990	
POMGnT1 KO (laminin-111)	5.385	0.548	8.900 ± 0.976	0.049
Wildtype (perlecan)	5.716	0.514	7.435 ± 1.045	
POMGnT1 KO (perlecan)	3.732	0.786	3.783 ± 0.886	0.047

Abbreviations: B_{max}, maximal immunofluorescence intensity; KO, knockout; SEM, standard error of the mean; $T_{1/2}$, time to reach 50% maximal immunofluorescence intensity; $V_{initial}$, initial rate of fluorescence increase. All p values are comparisons of knockout samples with corresponding wildtype controls.

Table II

Differential expression of BM components between Wildtype and POMGnT1 knockout ILMs.

	Fold change (Wildtype/POMGnT1 knockout)[a]	
Polypeptide	**Experiment 1**	**Experiment 2**
Laminin α-1	1.621****	1.01
Laminin γ-1	1.150***	1.116
Laminin β-2	1.064	1.159****
Laminin α-5	−1.235****	ND
Nidogen-1	1.199****	1.704****
Nidogen-2	ND	1.426***
Collagen α-1 (IV)	−1.085**	−1.211**
Collagen α-2 (IV)	−1.084	−1.197****
Perlecan	−1.236****	−1.004

[a] A positive number indicates that the protein is more abundant in the wildtype while a negative number indicates that the protein is more abundant in the knockout.

ND= not detected

** $p<0.05$

*** $p<0.01$

**** $p<0.001$